Ferromagnetism of transition metals and screened exchange interactions

Y. Kakehashi* and M. Atiqur R. Patoary
Department of Physics and Earth Sciences, Faculty of Science,
University of the Ryukyus, 1 Senbaru, Nishihara, Okinawa, 903-0213, Japan
(Dated: January 18, 2013)

We have investigated the magnetic properties of Fe, Co, and Ni at finite temperatures on the basis of the first-principles dynamical coherent potential approximation (CPA) in order to clarify the role of the exchange interaction energy (J) screened by *sp* electrons and its applicability to finite-temperature magnetism. With use of the atomic J, we obtained the Curie temperatures ($T_{\rm C}$) 1930 K for Fe and 2550 K for fcc Co, which are overestimated by a factor of 1.8 as compared with the experimental values, while we obtained $T_{\rm C}$ = 620 K for Ni being in good agreement with the experiment. Calculated effective Bohr magneton numbers also quantitatively agree with the experimental values. By comparing the results with those obtained by the screened J and by comparing them with the experiments, we found that the screened J, which are reduced by 30% as compared with the atomic ones, improve the ground-state magnetizations and densities of states at low temperatures in Fe and fcc Co, as well as $T_{\rm C}$ in fcc Co. But the screened J yield worse results for finite temperature properties of Fe and underestimate both the ground-state magnetization and $T_{\rm C}$ in case of Ni. We discuss possible origins for these inconsistencies.

INTRODUCTION

The band theory of itinerant magnetism has been much developed in the past half a century on the basis of the density functional theory (DFT) [1–3] with local spin density approximation (LSDA) [4] or the generalized gradient approximation (GGA) [5]. The DFT explains quantitatively the ground-state magnetism of 3*d* transition metals and alloys. The first-principles band calculations with use of the LSDA, for example, yield the magnetization per atom 2.15 $\mu_{\rm B}$ for Fe and 0.59 $\mu_{\rm B}$ for Ni, which are in good agreement with the experimental values [6, 7] 2.22 $\mu_{\rm B}$ and 0.62 $\mu_{\rm B}$, respectively. The LSDA stabilizes artificially the fcc Fe instead of the bcc Fe with the volume contraction by 15 %. The GGA has solved the problem on the stability of structure in Fe [8].

On the other hand, understanding of the finite-temperature magnetism in transition metals is still far from the final goal of quantitative description. The Stoner theory based on the DFT band calculations yields the Curie temperatures ($T_{\rm C}$), 6000 K for Fe and 3000 K for Ni [9, 10], which are 6 or 5 times as large as the observed values (1040 K for Fe [11] and 630 K for Ni [12]). Because of a large discrepancy between the theory and the experiment, many theories which take into account spin fluctuations at finite temperatures have been developed [13]. Hubbard [14] and Hasegawa [15] proposed a single-site spin fluctuation theory (SSF) on the basis of the functional integral method [16–19] and the coherent potential approximation (CPA) [20, 21]. They explained the Curie-Weiss susceptibility in 3*d* transition metals and obtained the Curie temperatures in Fe and Ni which qualitatively agree with the experiments.

The SSF, however, reduces to the Hartree-Fock theory at $T = 0$ because it is based on a high-temperature approximation. Therefore, the theory does not take into account electron correlations at the ground state as discussed by Gutzwiller [22–24], Hubbard [25, 26], and Kanamori [27]. Kakehashi and Fulde [28] proposed a variational theory at finite temperatures which takes into account the Gutzwiller-type electron correlations at the ground state and reduces to the SSF at high temperatures. They found that the Curie temperatures in Fe and Ni are reduced by 30% $\sim$ 50% due to correlated motion of electrons. Hasegawa [29] also proposed a similar theory on the basis of the slave-boson functional integral method. These theories are not suitable for systematic improvements of the theory because of the difficulty in finding a suitable temperature dependence of the effective potential being projected onto the static fields. In order to make a systematic improvements possible, we proposed the dynamical CPA [30] which fully takes into account the single-site spin and charge fluctuations self-consistently, and clarified the basic properties of the theory with use of a Monte-Carlo method. In the next paper [31] which we refer to I, we proposed more analytic method to the dynamical CPA using the harmonic approximation (HA) [32, 33].

Towards quantitative calculations, it is indispensable to take into account realistic band structures in solids. In our recent paper [34] which we refer to II, we proposed the first-principles dynamical CPA combining the dynamical CPA+HA with the LDA+U scheme [35] based on the tight-binding linear muffin-tin orbitals (TB-LMTO) [36]. Quite recently we extended the calculations taking into account the dynamical corrections up to the 4th or-

der in Coulomb interactions, and have shown that the single-particle excitation spectra obtained by the first-principles dynamical CPA explain systematic change of the X-ray photoemission spectroscopy (XPS) and the bremsstrahlung isochromat (BIS) data from Sc to Cu at high-temperatures [37, 38].

In our numerical calculations, we adopted the Coulomb interactions U obtained by Anisimov *et. al.* [39], and by Bandyopadhyay and Sarma [40]. The exchange interaction energies J were taken from the values obtained by the Hartree-Fock atomic calculations [41]. Recently, considerable efforts to obtain the first-principles U and J have been made at the ground state. Aryasetiawan and coworkers [42] obtained the Coulomb and exchange interactions for d orbitals which are screened by sp electrons, using the random phase approximation (RPA) and the LMTO method. The same type of calculations has been performed by using the first-principles Wannier orbitals by Miyake and Aryasetiawan [43]. These results indicate that irrespective of transition metal elements the exchange energy integral J are reduced by about 30% as compared with the atomic ones. Although the methods have been applied to many other compounds [44], there is no systematic investigation for the influence of the screened J on magnetic properties.

We investigate in this paper the ferromagnetic properties of Fe, Co, and Ni on the basis of the first-principle dynamical CPA using both the atomic exchange interaction energies (atomic J) and the exchange interaction energies screened by 30% (screened J). We examine the role of the exchange energy parameters in the magnetic properties at finite temperatures and clarify their validity to the magnetic properties. We will demonstrate that use of the screened J does not necessary improve theoretical results at finite temperatures, though we find some improvements at low temperature regime.

As we have proven in our previous papers [13, 45], the dynamical CPA is equivalent to the many-body CPA [46] in disordered alloys, the dynamical mean-field theory (DMFT) [47–51] in the metal-insulator transitions, and the projection operator CPA [52] for excitation problem in solids. The first-principles DMFT calculations for Fe and Ni have been performed at the ground state by Miura and Fujiwara [53] within the iterative perturbation method. The finite-temperature DMFT calculations for Fe and Ni have been performed by using the Hamiltonian without transverse spin fluctuations [54]. In both cases, atomic exchange interaction energy $J = 0.066$ Ry was adopted for Fe and Ni. We present here the finite-temperature results obtained by the Hamiltonian with transverse spin fluctuations and by using both the atomic J and the screened J values.

The outline of the paper is as follows. In the following section, we summarize the first-principles dynamical CPA based on the HA. In Sec. III, we present numerical results of calculations for the densities of states as the excitation spectra, magnetization vs temperature curves, Curie temperatures, paramagnetic susceptibilities, effective Bohr magneton numbers, as well as the amplitudes of local magnetic moments in Fe, Co, and Ni. By comparing these quantities calculated by the atomic J with those obtained by the screened J, we will clarify the role of the screening effects on the exchange energy J, and discuss the availability of the screened J. Furthermore, we discuss the validity of the screened J by comparing calculated magnetic properties with those in experiments. In Sec. IV, we present a summary of our works, and discuss possible reasons for the disagreement with experiments when the screened J are applied.

FIRST-PRINCIPLES DYNAMICAL CPA

In the first-principles dynamical CPA, we adopt the TB-LMTO Hamiltonian combined with a LDA+U Coulomb interactions as follows [34].

$$H = H_0 + H_1, \tag{1}$$

$$H_0 = \sum_{iL\sigma} (\epsilon_L^0 - \mu)\, \hat{n}_{iL\sigma} + \sum_{iLjL'\sigma} t_{iLjL'}\, a^\dagger_{iL\sigma} a_{jL'\sigma}\ , \tag{2}$$

$$\begin{aligned} H_1 \ = \ & \sum_i \Big[\sum_m U_0\, \hat{n}_{ilm\uparrow}\hat{n}_{ilm\downarrow} + \sum_{m>m'} (U_1 - \frac{1}{2}J)\hat{n}_{ilm}\hat{n}_{ilm'} \\ & - \sum_{m>m'} J\hat{\boldsymbol{s}}_{ilm}\cdot\hat{\boldsymbol{s}}_{ilm'} \Big]\ . \end{aligned} \tag{3}$$

We assumed here a transition metal with an atom per unit cell. ϵ_L^0 in Eq. (2) is an atomic level on site i and orbital L, μ is the chemical potential, $t_{iLjL'}$ is a transfer integral between orbitals iL and jL'. $L = (l, m)$ denotes s, p, and d orbitals. $a^\dagger_{iL\sigma}$ ($a_{iL\sigma}$) is the creation (annihilation) operator for an electron with orbital L and spin σ on site i, and $\hat{n}_{iL\sigma} = a^\dagger_{iL\sigma}a_{iL\sigma}$ is a charge density operator for electrons with orbital L and spin σ on site i.

The Coulomb interaction term H_1 in Eq. (3) consists of the on-site interactions between d electrons ($l = 2$). U_0 (U_1) and J denote the intra-orbital (inter-orbital) Coulomb and exchange interactions, respectively. $\hat{n}_{ilm}$ ($\hat{\boldsymbol{s}}_{ilm}$) with $l = 2$ is the charge (spin) density operator for d electrons on site i and orbital m. Note that the atomic level ϵ_L^0 in H_0 is not identical with the LDA atomic level ϵ_L; $\epsilon_L^0 = \epsilon_L - \partial E^U_{\rm LDA}/\partial n_{iL\sigma}$. Here $n_{iL\sigma}$ is the charge density at the ground state, $E^U_{\rm LDA}$ is a LDA functional to the intra-atomic Coulomb interactions [35, 39].

In the dynamical CPA, we transform in the free energy the interacting Hamiltonian H_1 into a one-body Hamiltonian with dynamical potential v for time-dependent random charge and exchange fields, using the functional integral method [19, 34]. Introducing a site-diagonal uniform medium, *i.e.*, a coherent potential Σ into the potential part, we expand the correction $v - \Sigma$ with respect to

sites in the free energy. The zeroth term in the expansion is the free energy for a uniform medium, $\tilde{\mathcal{F}}[\Sigma]$. The next term is an impurity contribution to the free energy. The dynamical CPA neglects the higher-order terms associated with inter-site correlations. The free energy per atom is then given by [31, 34]

$$\mathcal{F}_{\rm CPA} = \tilde{\mathcal{F}}[\Sigma] - \beta^{-1}\ln \int \Big[\prod_{\alpha}\sqrt{\frac{\beta\tilde{J}_\alpha}{4\pi}}d\xi_\alpha\Big]\,{\rm e}^{-\beta E_{\rm eff}(\boldsymbol{\xi})}. \quad (4)$$

Here β is the inverse temperature, $\tilde{J}_x = \tilde{J}_y = \tilde{J}_\perp = [1-1/(2l+1)]J$, $\tilde{J}_z = U_0/(2l+1)+\tilde{J}_\perp$, and $\boldsymbol{\xi} = (\xi_x, \xi_y, \xi_z)$ is a static field variable on a site.

The effective potential $E_{\rm eff}(\boldsymbol{\xi})$ in Eq. (4) consists of the static term $E_{\rm st}(\boldsymbol{\xi})$ and the dynamical correction term $E_{\rm dyn}(\boldsymbol{\xi})$ as follows.

$$E_{\rm eff}(\boldsymbol{\xi}) = E_{\rm st}(\boldsymbol{\xi}) + E_{\rm dyn}(\boldsymbol{\xi}). \quad (5)$$

The static term is given as

$$\begin{aligned} E_{\rm st}(\boldsymbol{\xi}) \;=\; & -\frac{1}{\beta}\sum_{mn}\ln\Big[(1-\delta v_{L\uparrow}(0)F_{L\uparrow}(i\omega_n))(1-\delta v_{L\downarrow}(0)F_{L\downarrow}(i\omega_n)) - \frac{1}{4}\tilde{J}_\perp^2\xi_\perp^2 F_{L\uparrow}(i\omega_n)F_{L\downarrow}(i\omega_n)\Big] \\ & +\frac{1}{4}\Big[-(U_0-2U_1+J)\sum_m \tilde{n}_L(\boldsymbol{\xi})^2 - (2U_1-J)\tilde{n}_l(\boldsymbol{\xi})^2 + \tilde{J}_\perp^2\xi_\perp^2 + \tilde{J}_z^2\xi_z^2\Big]. \end{aligned} \quad (6)$$

Here $\delta v_{L\sigma}(0) = v_{L\sigma}(0) - \Sigma_{L\sigma}(i\omega_n)$, and $\xi_\perp^2 = \xi_x^2 + \xi_y^2$. $v_{L\sigma}(0)$ is a static potential given by $v_{L\sigma}(0) = [(U_0 - 2U_1 + J)\tilde{n}_{lm}(\boldsymbol{\xi}) + (2U_1 - J)\tilde{n}_l(\boldsymbol{\xi})]/2 - \tilde{J}_z\xi_z\sigma/2$, $\Sigma_{L\sigma}(i\omega_n)$ is the coherent potential for Matsubara frequency $\omega_n = (2n+1)\pi/\beta$. The electron number $\tilde{n}_L(\boldsymbol{\xi})$ for a given $\boldsymbol{\xi}$ is expressed by means of an impurity Green function as

$$\tilde{n}_L(\boldsymbol{\xi}) = \frac{1}{\beta}\sum_{n\sigma} G_{L\sigma}(\boldsymbol{\xi}, i\omega_n), \quad (7)$$

and $\tilde{n}_l(\boldsymbol{\xi}) = \sum_m \tilde{n}_L(\boldsymbol{\xi})$. The impurity Green function $G_{L\sigma}(\boldsymbol{\xi}, i\omega_n)$ has to be determined self-consistently. The explicit expression will be given later (see Eq. (32)).

The coherent Green function $F_{L\sigma}(i\omega_n)$ in Eq. (6) is defined by

$$F_{L\sigma}(i\omega_n) = [(i\omega_n - \boldsymbol{H}_0 - \boldsymbol{\Sigma}(i\omega_n))^{-1}]_{iL\sigma iL\sigma}. \quad (8)$$

Here $(\boldsymbol{H}_0)_{iL\sigma jL'\sigma}$ is the one-electron Hamiltonian matrix for the noninteracting Hamiltonian H_0, and $(\boldsymbol{\Sigma}(i\omega_n))_{iL\sigma jL'\sigma} = \Sigma_{L\sigma}(i\omega_n)\delta_{ij}\delta_{LL'}$.

The dynamical potential $E_{\rm dyn}(\boldsymbol{\xi})$ in Eq. (5) has been obtained within the harmonic approximation (HA) [31–34]. It is based on an expansion of $E_{\rm dyn}(\boldsymbol{\xi})$ with respect to the frequency mode of the dynamical potential $v_{L\sigma\sigma'}(i\omega_\nu)$, where $\omega_\nu = 2\nu\pi/\beta$. The HA is the neglect of the mode-mode coupling terms in the expansion. We have then

$$E_{\rm dyn}(\boldsymbol{\xi}) = -\beta^{-1}\ln\left[1 + \sum_{\nu=1}^{\infty}(\overline{D}_\nu - 1)\right]. \quad (9)$$

Here the determinant D_ν is a contribution from a dynamical potential $v_{L\sigma\sigma'}(i\omega_\nu)$ with frequency ω_ν, and the upper bar denotes a Gaussian average with respect to the dynamical charge and exchange field variables, $\zeta_m(i\omega_n)$ and $\xi_{m\alpha}(i\omega_n)$ $(\alpha = x, y, z)$.

The determinant D_ν is expressed as [34]

$$D_\nu = \prod_{k=0}^{\nu-1}\left[\prod_{m=1}^{2l+1} D_\nu(k,m)\right], \quad (10)$$

$$D_\nu(k,m) = \begin{vmatrix} \ddots & & & & & \\ 1 & 1 & & 0 & & \\ a_{-\nu+k}(\nu,m) & 1 & 1 & & & \\ & a_k(\nu,m) & 1 & 1 & & \\ & & a_{\nu+k}(\nu,m) & 1 & 1 & \\ 0 & & & a_{2\nu+k}(\nu,m) & & \\ & & & & & \ddots \end{vmatrix}. \quad (11)$$

Note that 1 in the above determinant denotes the 2×2 unit matrix, $a_n(\nu,m)$ is a 2×2 matrix in the spin space, which are defined by

$$\begin{aligned} a_n(\nu,m)_{\sigma\sigma'} \;=\; & \sum_{\sigma''\sigma'''\sigma''''} v_{L\sigma\sigma''}(i\omega_\nu)\tilde{g}_{L\sigma''\sigma'''}(i\omega_n - i\omega_\nu) \\ & \times v_{L\sigma'''\sigma''''}(-i\omega_\nu)\tilde{g}_{L\sigma''''\sigma'}(i\omega_n)\ , \end{aligned} \quad (12)$$

$$\begin{aligned} v_{L\sigma\sigma'}(i\omega_\nu) \;=\; & -\frac{1}{2}\sum_{m'} iA_{mm'}\zeta_{m'}(i\omega_\nu)\delta_{l2}\delta_{\sigma\sigma'} \\ & -\frac{1}{2}\sum_{\alpha}\sum_{m'} B^\alpha_{mm'}\xi_{m'\alpha}(i\omega_\nu)\delta_{l2}(\sigma_\alpha)_{\sigma\sigma'}\ , \end{aligned} \quad (13)$$

$$\tilde{g}_{L\sigma\sigma'}(i\omega_n) = [(F_L(i\omega_n)^{-1} - \delta v_0)^{-1}]_{\sigma\sigma'}\ . \quad (14)$$

Here σ_α ($\alpha = x, y, z$) are the Pauli spin matrices. $A_{mm'} = U_0\delta_{mm'} + (2U_1 - J)(1 - \delta_{mm'})$, $B^\alpha_{mm'} = J(1 - \delta_{mm'})$ ($\alpha = x, y$), and $B^z_{mm'} = U_0\delta_{mm'} + J(1 - \delta_{mm'})$. $\tilde{g}_{L\sigma\sigma'}(i\omega_n)$ is the impurity Green function in the static approximation, $(F_L(i\omega_n))_{\sigma\sigma'} = F_{L\sigma}(i\omega_n)\delta_{\sigma\sigma'}$, and δv_0 is defined by $(\delta v_0)_{\sigma\sigma'} = v_{L\sigma\sigma'}(0) - \Sigma_{L\sigma}(i\omega_n)\delta_{\sigma\sigma'}$.

The determinant $D_\nu(k, m)$ defined by Eq. (11) is expanded with respect to the dynamical potential as follows.

$$D_\nu(k, m) = 1 + D^{(1)}_\nu(k, m) + D^{(2)}_\nu(k, m) + \cdots , \quad (15)$$

$$D^{(n)}_\nu(k, m) = \sum_{\alpha_1\gamma_1\cdots\alpha_n\gamma_n} v_{\alpha_1}(\nu, m)v_{\gamma_1}(-\nu, m)\cdots \times v_{\alpha_n}(\nu, m)v_{\gamma_n}(-\nu, m)\hat{D}^{(n)}_{\{\alpha\gamma\}}(\nu, k, m) . \quad (16)$$

Here the subscripts α_i and γ_i take 4 values 0, x, y, and z, and

$$v_0(\nu, m) = -\frac{1}{2}i\sum_{m'} A_{mm'}\zeta_{m'}(i\omega_\nu)\delta_{l2} , \quad (17)$$

$$v_\alpha(\nu, m) = -\frac{1}{2}\sum_{m'} B^\alpha_{mm'}\xi_{m'\alpha}(i\omega_\nu)\delta_{l2} , \quad (\alpha = x, y, z) . \quad (18)$$

Note that the subscript $\{\alpha\gamma\}$ of $\hat{D}^{(n)}_{\{\alpha\gamma\}}(\nu, k, m)$ in Eq. (16) denotes a set of $(\alpha_1\gamma_1, \cdots, \alpha_n\gamma_n)$.

Substituting Eq. (15) into Eq. (10) and taking the Gaussian average, we reach

$$E_{\rm dyn}(\boldsymbol{\xi}) = -\beta^{-1}\ln\left(1 + \sum_{n=1}^{\infty}\sum_{\nu=1}^{\infty}\overline{D}^{(n)}_\nu\right), \quad (19)$$

and

$$\overline{D}^{(n)}_\nu = \frac{1}{(2\beta)^n}\sum_{\sum_{km} l(k,m)=n}\sum_{\{\alpha_j(k,m)\}}\sum_{\rm P}\prod_{m=1}^{2l+1}\prod_{k=0}^{\nu-1} \times\left[\Big(\prod_{j=1}^{l(k,m)} C^{\alpha_j(k,m)}_{mm_{\rm P}}\Big)\hat{D}^{(l(k,m))}_{\{\alpha\alpha_{\rm P^{-1}}\}}(\nu, k, m)\right]. \quad (20)$$

Here each element of $\{l(k, m)\}$ ($k = 0, \cdots, \nu - 1, m = 1, \cdots, 2l + 1$) has a value of zero or positive integer. $\alpha_j(k, m)$ takes one of 4 cases 0, x, y, and z. j denotes the j-th member of the (k, m) block with $l(k, m)$ elements. P denotes a permutation of a set $\{(j, k, m)\}$; $\mathrm{P}\{(j, k, m)\} = \{(j_{\rm P}, k_{\rm P}, m_{\rm P})\}$. $\alpha_{\rm P^{-1}}$ means a rearrangement of $\{\alpha_j(k, m)\}$ according to the inverse permutation P^{-1}. The coefficient $C^\alpha_{mm'}$ in Eq. (20) is a Coulomb interaction defined by

$$C^\alpha_{mm'} = \begin{cases} -A_{mm'} & (\alpha = 0) \\ B^\alpha_{mm'} & (\alpha = x, y, z) . \end{cases} \quad (21)$$

The frequency dependent factors $\hat{D}^{(n)}_{\{\alpha\gamma\}}(\nu, k, m)$ in Eqs. (16) and (20) consist of a linear combination of $2n$ products of the static Green functions. Their first few terms have been given in Appendix A of our paper II [34].

In the calculations of the higher-order dynamical corrections [38] $\hat{D}^{(n)}_{\{\alpha\gamma\}}(\nu, k, m)$, we note that the coupling constants $B^x_{mm'} = B^y_{mm'} = J(1 - \delta_{mm'})$ are considerably smaller than $A_{mm'}$ and $B^z_{mm'}$ because U_0 and $U_1 \gg J$. Thus we neglect the transverse potentials, $v_x(\nu, m)$ and $v_y(\nu, m)$. The approximation implies that $a_n(\nu, m)_{\sigma-\sigma} = 0$. The determinant $D_\nu(k, m)$ in Eq. (10) is then written by the products of the single-spin components as

$$D_\nu(k, m) = D_{\nu\uparrow}(k, m)D_{\nu\downarrow}(k, m). \quad (22)$$

Here $D_{\nu\sigma}(k, m)$ is defined by Eq. (11) in which the 2×2 unit matrices have been replaced by 1 (*i.e.*, 1×1 unit matrices), and the 2×2 matrices $a_n(\nu, m)$ have been replaced by the 1×1 matrices $a_n(\nu, m)_{\sigma\sigma}$. The latter is given by

$$a_n(\nu, m)_{\sigma\sigma} = \sum_{\alpha,\gamma}^{0,z} v_\alpha(\nu, m)v_\gamma(-\nu, m)\hat{h}_{\alpha\gamma\sigma}e_{n\sigma}(\nu, m), \quad (23)$$

$$e_{n\sigma}(\nu, m) = \tilde{g}_{L\sigma}(n - \nu)\tilde{g}_{L\sigma}(n). \quad (24)$$

Here $\hat{h}_{\alpha\gamma\sigma} = \delta_{\alpha\gamma} + \sigma(1 - \delta_{\alpha\gamma})$, and we used a notation $\tilde{g}_{L\sigma}(n) = \tilde{g}_{L\sigma\sigma}(i\omega_n)$ for simplicity.

In order to reduce these summations, we make use of an asymptotic approximation [31, 38].

$$e_{n\sigma}(\nu, m) \sim \overline{q}_\nu\left(\tilde{g}_{L\sigma}(n - \nu) - \tilde{g}_{L\sigma}(n)\right) , \quad (25)$$

where $\overline{q}_\nu = \beta/2\pi\nu i$. The approximation is justified in the high-frequency limit where $\tilde{g}_{L\sigma}(n)$ is written as

$$\tilde{g}_{L\sigma}(n) = \frac{1}{i\omega_n - \epsilon^0_L + \mu - v_{L\sigma}(0)} + O\left(\frac{1}{(i\omega_n)^3}\right). \quad (26)$$

In the asymptotic approximation, we obtain

$$\hat{D}^{(n)}_{\{\alpha\gamma\}}(\nu, k, m) = \sum_{l=0}^{n}\hat{D}^{(l)}_{\{\alpha_1\gamma_1\cdots\alpha_l\gamma_l\}\uparrow}(\nu, k, m) \times\hat{D}^{(n-l)}_{\{\alpha_{l+1}\gamma_{l+1}\cdots\alpha_n\gamma_n\}\downarrow}(\nu, k, m) . \quad (27)$$

Here we wrote the subscript at the r.h.s. (right-hand-side) explicitly to avoid confusion. Note that the values of α_i and γ_i are limited to 0 or z in the present approximation. The spin-dependent quantities are given by [38]

$$\hat{D}^{(l)}_{\{\alpha\gamma\}\sigma}(\nu, k, m) = \Lambda^{(l)}_\sigma(\{\alpha\gamma\})\frac{\overline{q}^i_\nu}{l!}B^{(l)}_\sigma(\nu, k, m) , \quad (28)$$

$$\Lambda^{(l)}_\sigma(\{\alpha\gamma\}) = \begin{cases} 1 & (\sigma = \uparrow) \\ (-1)^{l-n_l(\{\alpha\gamma\})} & (\sigma = \downarrow) \end{cases} , \quad (29)$$

$$B_{\sigma}^{(l)}(\nu,k,m)=\Big[\prod_{j=0}^{l-1}\tilde{g}_{L\sigma}(j\nu+k)\Big]+\sum_{i=0}^{l-1}\frac{(-)^{l-i}l!}{i!(l-i)!}\Big[\prod_{j=-(l-i)}^{i-1}\tilde{g}_{L\sigma}(j\nu+k)\Big]\Big[1+\frac{l-i}{\overline{q}_{\nu}^{i}}\tilde{g}_{L\sigma}(i\nu+k)\Big]\ . \tag{30}$$

Here $\hat{D}^{(0)}_{\{\alpha\gamma\}\sigma}(\nu,k,m)=1$. $n_l(\{\alpha\gamma\})$ is the number of $\{\alpha_i\gamma_i\}$ pairs such that $\alpha_i=\gamma_i$ among the l pairs. Equation (30) reduces to the result of the zeroth asymptotic approximation in our paper I [31] when there is no orbital degeneracy.

In the actual applications we make use of the exact form up to a certain order of expansion in $\overline{D}_{\nu}^{(m)}$ (see Eq. (15)), and for higher-order terms we adopt an asymptotic form (27). In this way, we can take into account dynamical corrections systematically starting from both sides of the weak-interaction limit and the high-temperature limit.

The coherent potential can be determined by the stationary condition $\delta\mathcal{F}_{\rm CPA}/\delta\Sigma=0$. This yields the dynamical CPA equation as [34]

$$\langle G_{L\sigma}(\boldsymbol{\xi},i\omega_n)\rangle=F_{L\sigma}(i\omega_n)\ . \tag{31}$$

Here $\langle\ \rangle$ at the l.h.s. (left-hand-side) is a classical average taken with respect to the effective potential $E_{\rm eff}(\boldsymbol{\xi})$. The impurity Green function is given by

$$G_{L\sigma}(\boldsymbol{\xi},i\omega_l)=\tilde{g}_{L\sigma\sigma}(i\omega_l)+\frac{\sum_n\sum_{\nu}\frac{\delta\overline{D}_{\nu}^{(n)}}{\kappa_{L\sigma}(i\omega_l)\delta\Sigma_{L\sigma}(i\omega_l)}}{1+\sum_n\sum_{\nu}\overline{D}_{\nu}^{(n)}}\ . \tag{32}$$

The first term at the r.h.s. is the impurity Green function in the static approximation, which is given by Eq. (14). The second term is the dynamical corrections, and $\kappa_{L\sigma}(i\omega_l)=1-F_{L\sigma}(i\omega_l)^{-2}\delta F_{L\sigma}(i\omega_l)/\delta\Sigma_{L\sigma}(i\omega_l)$.

Solving the CPA equation (31) self-consistently, we obtain the effective medium. The electron number on each orbital L is then calculated from

$$\langle\hat{n}_L\rangle=\frac{1}{\beta}\sum_{n\sigma}F_{L\sigma}(i\omega_n)\ . \tag{33}$$

The chemical potential μ is determined from the condition $n_e=\sum_L\langle\hat{n}_L\rangle$. Here n_e denotes the conduction electron number per atom. The magnetic moment is given by

$$\langle\hat{m}_L^z\rangle=\frac{1}{\beta}\sum_{n\sigma}\sigma F_{L\sigma}(i\omega_n)\ . \tag{34}$$

In particular, the $l=2$ component of magnetic moment is expressed as

$$\langle\hat{\boldsymbol{m}}_l\rangle=\langle\boldsymbol{\xi}\rangle\ . \tag{35}$$

The above relation implies that the effective potential $E_{\rm eff}(\boldsymbol{\xi})$ is a potential energy for a local magnetic moment $\boldsymbol{\xi}$.

In the numerical calculations, we took into account the dynamical corrections up to the second order ($n\le 2$) exactly, and the higher-order terms up to the fourth order within the asymptotic approximation. Summation with respect to ν in Eqs. (19) and (32) was taken up to $\nu=100$ for $n=1$ and 2, and up to $\nu=2$ for $n=3,\ 4$.

When we solve the CPA equation (31), we adopted a decoupling approximation to the thermal average of impurity Green function [55] for simplicity, *i.e.*,

$$\langle G_{L\sigma}(\xi_z,\xi_{\perp}^2,i\omega_n)\rangle\ =\ \sum_{q=\pm}\frac{1}{2}\left(1+q\frac{\langle\xi_z\rangle}{\sqrt{\langle\xi_z^2\rangle}}\right)\times G_{L\sigma}(q\sqrt{\langle\xi_z^2\rangle},\langle\xi_{\perp}^2\rangle,i\omega_n)\ . \tag{36}$$

Here we wrote the static exchange field $\boldsymbol{\xi}$ as $(\xi_z,\xi_{\perp}^2)$ in order to make the decoupling approximation clearer. The approximation is correct up to the second moment (*i.e.*, $\langle\xi_{\alpha}^2\rangle$) and arrows us to describe the thermal spin fluctuations in a simpler way.

On the other hand, we adopted a diagonal approximation [56] to the coherent Green function at the r.h.s. of Eq. (31).

$$F_{L\sigma}(n)=\int\frac{\rho_L^{\rm LDA}(\epsilon)d\epsilon}{i\omega_n-\epsilon-\Sigma_{L\sigma}(i\omega_n)-\Delta\epsilon_L}\ . \tag{37}$$

Here $\rho_L^{\rm LDA}(\epsilon)$ is the local density of states for the LDA band calculation, and $\Delta\epsilon_L=(\epsilon_L-\epsilon_L^0)\delta_{l2}$. The approximation partly takes into account the effects of hybridization between different l blocks in the nonmagnetic state, but neglects the effects via spin polarization.

The CPA equation (31) with use of the decoupling approximation (36) yields an approximate solution to the full CPA equation. For the calculations of the single-particle densities of states, we adopted the following average t-matrix approximation [21, 57] (ATA) after we solved Eq. (31) with use of the decoupling approximation (36).

$$\Sigma_{L\sigma}^{\rm ATA}(i\omega_n)=\Sigma_{L\sigma}(i\omega_n)+\frac{\langle G_{L\sigma}(\xi_z,\xi_{\perp}^2,i\omega_n)\rangle-F_{L\sigma}(i\omega_n)}{\langle G_{L\sigma}(\xi_z,\xi_{\perp}^2,i\omega_n)\rangle F_{L\sigma}(i\omega_n)}\ . \tag{38}$$

Here the coherent potential in the decoupling approximation is used at the r.h.s., but the full average $\langle\ \rangle$ of the

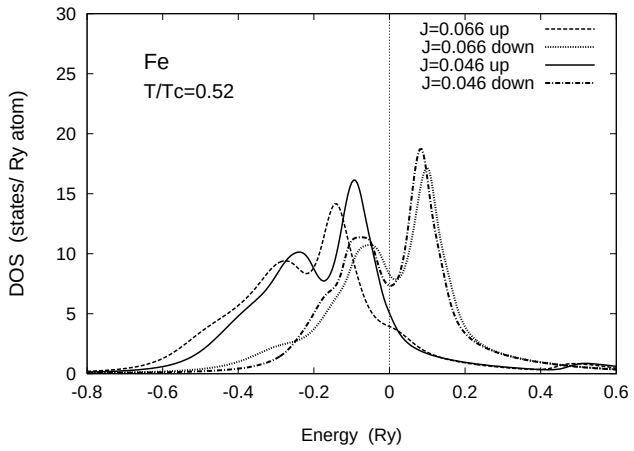

FIG. 1: Spin-resolved d densities of states (DOS) of Fe at $T/T_{\rm C} = 0.52$ for atomic J (dashed curve for the up-spin DOS, dotted curve for the down-spin DOS) and screened J (solid curve for the up-spin DOS, dot-dashed curve for the down-spin DOS).

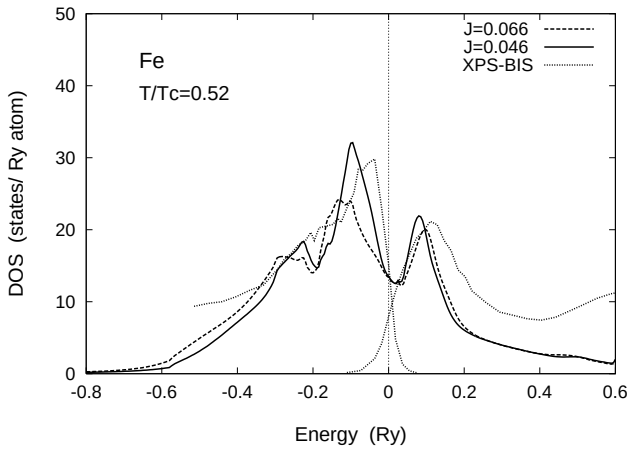

FIG. 2: Total DOS of Fe for atomic J (dashed curve) and screened J (solid curve) at $T/T_{\rm C} = 0.52$. The XPS [59] and BIS [60] data at room temperature are shown by dotted curves.

impurity Green function is taken. The ATA is a one-shot correction to the full CPA.

The coherent potential $\Sigma_{L\sigma}(z)$ on the real axis $z = \omega + i\delta$ is then calculated by using the Padé numerical analytic continuation method [58]. Here δ is an infinitesimal positive number. The densities of states (DOS) as the single-particle excitations, $\rho_{L\sigma}(\omega)$ are calculated from the relation,

$$\rho_{L\sigma}(\omega) = -\frac{1}{\pi} \mathrm{Im}\, F_{L\sigma}(z) \ . \tag{39}$$

NUMERICAL RESULTS

In the numerical calculations, we adopted the lattice constants used by Andersen *et. al.* [36], and performed the LDA calculations with use of the Barth-Hedin exchange-correlation potential to make the TB-LMTO Hamiltonian (2). For Fe and Ni, we adopted average Coulomb interaction parameters $\overline{U}$ and the average exchange interactions $\overline{J}$ used by Anisimov *et. al.* [39], and for Co we adopted $\overline{U}$ obtained by Bandyopadhyay *et. al.* [40] and $\overline{J}$ obtained by the Hartree-Fock atomic calculations [41] ; $\overline{U} = 0.169$ Ry and $\overline{J} = 0.066$ Ry for Fe, $\overline{U} = 0.245$ Ry and $\overline{J} = 0.069$ Ry for fcc Co, and $\overline{U} = 0.221$ Ry and $\overline{J} = 0.066$ Ry for Ni. The exchange interaction energies mentioned above are basically atomic ones. As for the screened exchange interaction energy, we adopted 70% values [42, 43] of these atomic $\overline{J}$; $\overline{J} = 0.046$ Ry for Fe, $\overline{J} = 0.048$ Ry for fcc Co, and $\overline{J} = 0.046$ Ry for Ni. The intra-orbital Coulomb interaction U_0, inter-orbital Coulomb interaction U_1, and the exchange interaction energy parameter J were calculated from $\overline{U}$ and $\overline{J}$ as $U_0 = \overline{U} + 8\overline{J}/5$, $U_1 = \overline{U} - 2\overline{J}/5$, and $J = \overline{J}$, using the relation $U_0 = U_1 + 2J$.

We present in Fig. 1 the d densities of states (DOS) in the ferromagnetic Fe. In the case of atomic $J = 0.066$ Ry, the DOS for up-spin electrons consists of two peaks, the main peak due to e_g electrons at $\omega \approx -0.15$ Ry and the second peak due to t_{2g} electrons at $\omega \approx -0.30$ Ry. We also find small humps at $\omega \approx -0.5$ Ry and 0.0 Ry. These humps are caused by both e_g and t_{2g} electrons. The DOS for down-spin electrons also show the structure consisting of the main peak at $\omega = 0.1$ Ry mainly due to e_g electrons and the second peak at $\omega \approx -0.05$ Ry mainly due to t_{2g} electrons. We find a small hump at $\omega \approx -0.3$ Ry due to t_{2g} electrons.

When we adopt the screened $J = 0.046$ Ry, the peaks of the up-spin DOS shift up towards the Fermi level by about 0.05 Ry, and those of the down-spin DOS shift down. It indicates the reduction of the magnetization. The hump at $\omega \approx -0.5$ Ry shifts up and loses its weight, while the hump at $\omega \approx -0.3$ Ry disappears. Accordingly the spectral weights of the two peaks are enhanced. The disappearance of the humps implies that the humps originates in the multiplet excitations due to strong J. The resulting total DOS are shown in Fig. 2. The screened J enhances the main peak and shifts it to the Fermi level. The DOS obtained by the screened J seems to explain better the XPS data at room temperature [59].

Solving the CPA equation (31) self-consistently at each temperature, we obtain the magnetization vs temperature ($M - T$) curves for Fe as shown in Fig. 3. The ground-state magnetizations $M(0)$ obtained by an extrapolation of the $M-T$ curves are 2.58 $\mu_{\rm B}$ for $J = 0.066$ Ry and 2.39 $\mu_{\rm B}$ for $J = 0.046$ Ry. The latter is in better agreement with experimental value [6] 2.22 $\mu_{\rm B}$, though it is still somewhat overestimated. The reduction of $M(0)$

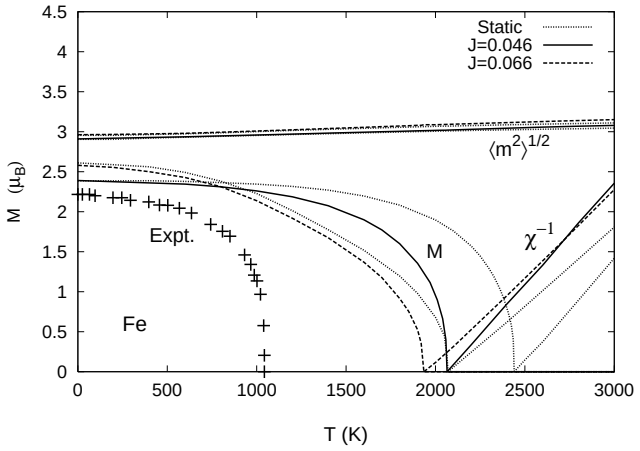

FIG. 3: Magnetization vs temperature ($M-T$) curves, inverse susceptibilities χ^{-1}, and amplitudes of local moments $\langle \boldsymbol{m}^2 \rangle^{1/2}$ of Fe for atomic J (dashed curves) and screened J (solid curves). Corresponding curves in the static approximation are drawn by dotted curves. The curve with higher (lower) $T_{\rm C}$ corresponds to the screened (atomic) J. Experimental data [61] of M are shown by +.

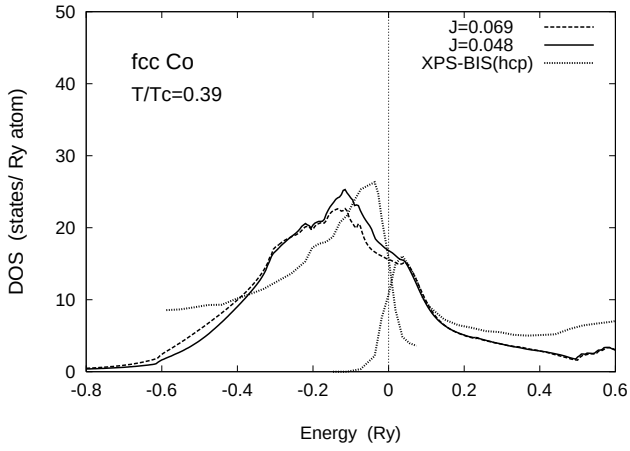

FIG. 4: Total DOS of fcc Co for atomic J (dashed curve) and screened J (solid curve) at $T/T_{\rm C}=0.39$. The XPS [59] and BIS [60] data at room temperature for hcp Co are shown by dotted curves.

with decreasing J is explained by the fact that the Hund-rule coupling J which parallels the spins of electrons in each atom competes with the disordering due to electron hopping and thus $M(0)$ is not saturated. We also find the reduction of the amplitude of local moment $\langle \boldsymbol{m}^2 \rangle^{1/2}$ by 0.066 $\mu_{\rm B}$ when the screened J is used, as seen in Fig. 3.

With increasing temperature, the magnetization for screened J shows less temperature dependence at low temperatures and rapidly decreases near $T_{\rm C}$. Resulting $T_{\rm C}$ is higher than that obtained by the atomic J. Basically the Curie temperature $T_{\rm C}$ is determined by the ratio of the magnetic energy to the magnetic entropy. The enhancement of $T_{\rm C}$ with reducing J in Fe is attributed to the reduction of the magnetic entropy with the collapse of the Hund rule coupling. Further reduction of J should decrease $T_{\rm C}$ because of the reduction of magnetic energy.

Calculated susceptibilities of Fe follow the Curie-Weiss law as shown in Fig. 3. We find the effective Bohr magneton numbers $m_{\rm eff}=3.0$ $\mu_{\rm B}$ for $J=0.066$ Ry and $m_{\rm eff}=2.8$ $\mu_{\rm B}$ for $J=0.046$ Ry, which are compared with the experimental value [62] 3.2 $\mu_{\rm B}$. The screened J underestimates the effective Bohr magneton number. We have also calculated the effective Bohr magneton number for fcc Fe at high temperatures (~ 2000 K), and obtained $m_{\rm eff}({\rm fcc})=4.2$ $\mu_{\rm B}$ for $J=0.066$ Ry and $m_{\rm eff}({\rm fcc})=2.6$ $\mu_{\rm B}$ for $J=0.046$ Ry after having included the volume effects on the susceptibilities. These values should be compared with the experimental value [63] 7.0 $\mu_{\rm B}$. The results again show that the screened J value underestimates $m_{\rm eff}$. Present results indicate that the high-temperature properties of Fe are explained better by the atomic J, while the low-temperature ones are explained by the screened J.

In the case of fcc Co, the d DOS for up-spin electrons shift up by 0.04 Ry and those for down-spin electrons shift down by 0.01 Ry when the atomic J is replaced by the screened J. The total DOS shifts towards the Fermi level and the peak at $\omega=-0.1$ Ry is considerably enhanced as shown in Fig. 4.

It should be noted that the XPS [59] and BIS [60] data are obtained for the hcp Co at room temperature, thus they are not able to be compared directly with the present results for fcc Co. Nevertheless, we find the peak position of the BIS data is in accordance with the hump position in the DOS. The band width of the DOS seems to be larger than that expected from the XPS data.

We present the magnetization vs temperature curves of fcc Co in Fig. 5. The ground-state magnetizations obtained by an extrapolation are 1.82 $\mu_{\rm B}$ for the atomic $J=0.069$ Ry and 1.72 $\mu_{\rm B}$ for the screened $J=0.048$ Ry, respectively; the latter obtained by the screened J is in better agreement with the experimental one [7] (1.74 $\mu_{\rm B}$). The amplitudes of local moments decrease by about 0.007 $\mu_{\rm B}$ with the reduction of the Hund-rule coupling by 0.021 Ry.

The magnetization for the screened J decreases in the same way as in the atomic J with increasing temperature (see Fig. 5). The calculated $T_{\rm C}$ is 2075 K for the screened $J=0.048$ Ry, and is smaller than $T_{\rm C}=2550$ K for atomic $J=0.069$ Ry. The former (latter) is 1.5 (1.8) times as large as the experimental value of fcc Co ($T_{\rm C}=1388$ K) [65]. We also calculated the susceptibilities. The inverse susceptibilities follow the Curie-Weiss law but show an upward convexity to some extent. Calculated effective Bohr magneton numbers are 3.0 $\mu_{\rm B}$ in both cases being in good agreement with the experimental value [62] 3.15 $\mu_{\rm B}$. They hardly change due to the

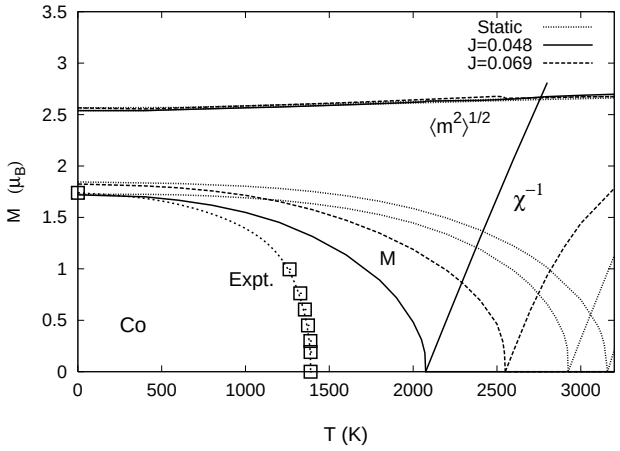

FIG. 5: Magnetization vs temperature ($M-T$) curves, inverse susceptibilities χ^{-1}, and amplitudes of local moments $\langle \boldsymbol{m}^2\rangle^{1/2}$ of fcc Co for atomic J (dashed curves) and screened J (solid curves). Corresponding curves in the static approximation are drawn by dotted curves. The curve with higher (lower) $T_{\rm C}$ corresponds to the atomic (screened) J. Experimental data [64] of M for fcc Co are shown by open squares and dashed line.

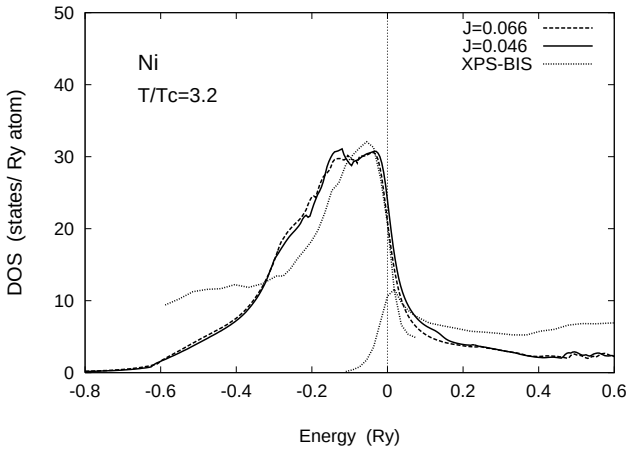

FIG. 6: Total DOS of Ni for atomic J (dashed curve) and screened J (solid curve) at $T/T_{\rm C} = 3.2$. The XPS [59] and BIS [60] data are shown by dotted curves.

reduction of J. These results indicate that effects of the Hund-rule coupling on the local magnetic moment are less significant as compared with the case of Fe because the number of d holes is rather small (about 2.36).

The DOS for Ni are presented in Fig. 6. They are shown for paramagnetic state because calculated $T_{\rm C}$ of Ni is lower than those in Fe and Co by a factor of 3 or 5, and the calculations of DOS at low temperatures below $T_{\rm C}$ are not easy in the present method with use of the numerical analytic continuation. The paramagnetic DOS are not sensitive to the choice of J since the Hund-rule coupling is not effective for the system with small number of d holes (≈ 1.32). Calculated d-band widths seem to be

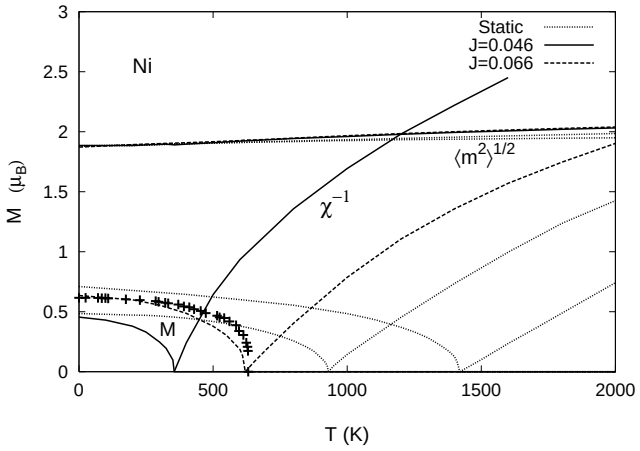

FIG. 7: Magnetization vs temperature ($M-T$) curves, inverse susceptibilities χ^{-1}, and amplitudes of local moments $\langle \boldsymbol{m}^2\rangle^{1/2}$ of Ni for atomic J (dashed curves) and screened J (solid curves). Corresponding curves in the static approximation are drawn by dotted curves. The curve with higher (lower) $T_{\rm C}$ corresponds to the atomic (screened) J. Experimental data [66] of M are shown by +.

somewhat larger than those expected from the XPS data. The same tendency was found also in fcc Co (see Fig. 4). The results suggest that the higher-order dynamical corrections are desired for the quantitative description of the DOS in these systems.

The magnetization vs temperature curves for Ni are presented in Fig. 7. The ground-state magnetization obtained by an extrapolation is 0.64 $\mu_{\rm B}$ for atomic J = 0.066 Ry and 0.46 $\mu_{\rm B}$ for screened $J = 0.046$ Ry. The experimental value [7] 0.62 $\mu_{\rm B}$ is in-between. The amplitude of local moment for $J = 0.066$ Ry is 1.93 $\mu_{\rm B}$, for example, at $T = T_{\rm C}$. The amplitude hardly changes even if the screened J is adopted. This is because the Hund-rule coupling is negligible for the system with small number of d holes.

The Curie temperatures in Ni are strongly reduced by the dynamical effects as shown in Fig. 7. We obtained $T_{\rm C} = 620$ K for the atomic J (=0.066 Ry) and 355 K for the screened J (= 0.046 Ry). The former is in good agreement with the observed $T_{\rm C} = 630$ K [12]. The screened J underestimates the Curie temperature. The results indicate that the value of J is significant for the spin polarization and the inter-site ferromagnetic coupling in Ni. In order to examine the ambiguity of the Coulomb interaction energy parameters, we performed the same calculations with use of different sets of (U, J): $(0.25, 0.073)$ Ry and (0.25, 0.051) Ry, where $U = 0.25$ Ry was obtained by Bandyopadhyay *et. al.* [40] and $J = 0.073$ Ry was taken from the Hartree-Fock atomic calculations [41]. We obtained $T_{\rm C} = 680$ K for the former (, *i.e.*, atomic J) and 325 K for the latter (, *i.e.*, screened J); the results are not so sensitive to the choice of U.

Calculated inverse susceptibilities are upwards convex,

being in agreement with the experimental data [62] for Ni. Effective Bohr magneton numbers calculated at $T \sim$ 2000 K are 1.6 $\mu_{\rm B}$ for both the screened and the atomic J. The results quantitatively agree with the experimental value [62] 1.6 $\mu_{\rm B}$.

SUMMARY

We have calculated the magnetic properties of Fe, Co, and Ni at finite temperatures on the basis of the first-principles dynamical CPA+HA, and investigated the effects of screened exchange interaction energy J on the magnetic properties in these ferromagnets.

When we apply the atomic J, we obtained from the magnetization vs temperature curves the Curie temperatures 1930K for Fe, 2550K for fcc Co, and 620K for Ni. Although calculated $T_{\rm C}$ in Ni is close to the experimental value [12] 630K, those in Fe and Co are overestimated by a factor of 1.8 as compared with the experimental values, 1040K (Fe) [11] and 1388K (Co) [65], respectively. In the present calculations using atomic J, the ground state magnetizations obtained by an extrapolation are 2.58 $\mu_{\rm B}$ (Fe), 1.82 $\mu_{\rm B}$ (fcc Co), and 0.64 $\mu_{\rm B}$ (Ni). Calculated magnetizations for Fe and fcc Co are considerably larger than the experimental values, 2.22 $\mu_{\rm B}$ (Fe) [6] and 1.74 $\mu_{\rm B}$ (Co) [7], while that for Ni agrees well with the experiment (0.62 $\mu_{\rm B}$). The results indicate that the atomic J overestimate the ferromagnetism of Fe and fcc Co at low temperatures. We have calculated the paramagnetic susceptibilities. Calculated effective Bohr magneton numbers, 3.0 $\mu_{\rm B}$ (Fe), 3.0 $\mu_{\rm B}$ (Co), and 1.6 $\mu_{\rm B}$ (Ni), quantitatively explain the experimental data.

The reduction of the exchange interaction energy by 30% due to screening by *sp* electrons weakens the Hund-rule coupling which builds up the local magnetic moment on each atom. We found that it reduces the ground-state magnetization $M(0)$ and the amplitudes of local moments in Fe and Co, especially the ground-state magnetizations 2.39 $\mu_{\rm B}$ (Fe) and 1.72 $\mu_{\rm B}$ (fcc Co) are in good agreement with the experiments. The screened J reduces the exchange splitting between the up and down DOS. The reduction of the splitting shifts the main peak in the spin-resolved DOS to the Fermi level and enhances the peak in case of Fe and Co. The screened J reduces the humps in the DOS below $T_{\rm C}$ which originate in the multiplet-type of excitations associated with J. The screened J also weakens the inter-site magnetic couplings. It reduces the magnetization in Ni, where the on-site Hund-rule coupling is not significant because of a small number of d holes.

With reducing J, the magnetic entropy and the magnetic energy decrease in general. We found that the 30% screened J enhances the Curie temperature $T_{\rm C}$ by 140 K in Fe because of the reduction of the magnetic entropy, while it reduces $T_{\rm C}$ in fcc Co by 480 K because of the reduction of the magnetic energy. The Curie temperatures of Fe and Co are overestimated by a factor of $1.5 \sim 2.0$ irrespective of the choice of J in the present calculations. It should be attiributed to the magnetic short range order which is not taken into account in the present theory. In the case of the susceptibilities, the screened J excessively reduces the effective Bohr magneton number in Fe where the Hund-rule coupling builds up the on-site magnetic moment.

By comparing both results of atomic J and screened J with the experimental data, we found that the screened J explains better the ground-state magnetization $M(0)$ and the DOS at low temperatures in case of Fe and Co. But it yields the underestimate of $M(0)$ in Ni. The atomic J seems to be better for the explanation of $M(0)$ in Ni. Concerning the finite-temperature properties, we found that the screened J improves the Curie temperature in Co, while the atomic J yields better $T_{\rm C}$ in case of Fe and Ni. The effective Bohr magneton numbers are quantitatively explained by the atomic J. The screened J underestimates $m_{\rm eff}$ for both the bcc and fcc Fe.

The above-mentioned results indicate that only for fcc Co the screened J seems to improve both the low- and the high-temperature properties. In the case of Fe, the high-temperature properties seem to be explained better by the atomic J, while the low-temperature ones by the screened J. In Ni, both the low- and the high-temperature properties are explained better by the atomic J.

Although we have to improve further the theory of dynamical CPA+HA at low-temperatures in order to obtain more solid conclusion, the present results obtained in the high-temperature region should be reasonable because the theory is an approach from the high-temperature limit and the magnetic short range order is not significant at high temperatures. The results for the effective Bohr magneton numbers indicate that one has to take into account the temperature dependence of J for the system like Fe where the Hund-rule coupling builds a large local magnetic moment but competes with the kinetic energy of d electrons. It is plausible that spin fluctuations at finite temperatures break the screening of J. The present results also suggest that the 30% screening of J is an overestimate for Ni. The range of applications of screened J and its validity have to be examined further in the future investigations with use of more advanced theories.

The present work is supported by Grant-in-Aid for Scientific Research (22540395). Numerical calculations have been partly carried out with use of the Hitachi SR11000 in the Supercomputer Center, Institute of Solid State Physics, University of Tokyo.

* yok@sci.u-ryukyu.ac.jp

[1] P. Hohenberg and W. Kohn, Phys. Rev. 136, B864 (1964).
[2] W. Kohn and L.J. Sham, Phys. Rev. 140, A1133 (1965).
[3] R.G. Parr and W. Yang, *Density Functional Theory of Atoms and Molecules* (Oxford University Press, Oxford, 1989).
[4] U. von Barth and L. Hedin, J. Phys. C **5**, 1629 (1972).
[5] J.P. Perdew and Y. Wang, Phys. Rev. B **33**, 8800 (1986). V.L. Moruzzi, J.F. Janak, and A.R. Williams, *Calculated Electronic Properties of Metals* (Pergamon Press, 1978).
[6] H. Danan, A. Herr, and A.J.P. Meyer, J. Appl. Phys. **39**, 669 (1968).
[7] M.J. Besnus, A.J.P. Meyer, and R. Berninger, Phys. Lett. **32 A**, 192 (1970).
[8] P. Bagno, O. Jepsen, and O. Gunnarsson, Phys. Rev. B 40, 1997 (1989).
[9] O. Gunnarson, Physica B **91**, 329 (1977).
[10] J.B. Staunton and B.L. Gyorffy, Phys. Rev. Lett. **69**, 371 (1992).
[11] A. Arrott and J.E. Noakes, Phys. Rev. Lett. **19**, 786 (1967).
[12] J.E. Noakes, N.E. Tornberg and A. Arrott, J. Appl. Phys. **37**, 1264 (1966).
[13] Y. Kakehashi, Adv. in Phys. **53**, 497 (2004); Phil. Mag. **86**, 2603 (2006).
[14] J. Hubbard, Phys. Rev. B **19**, 2626 (1979); **20**, 4584 (1979); **23**, 5974 (1981).
[15] H. Hasegawa, J. Phys. Soc. Jpn. **46**, 1504 (1979); **49**, 178 (1980).
[16] R. L. Stratonovich, Dokl. Akad. Nauk. SSSR **115**, 1097 (1958) [Sov. Phys. - Dokl. **2**, 416 (1958)].
[17] J. Hubbard, Phys. Rev. Lett. **3**, 77 (1959).
[18] W. E. Evenson, J. R. Schrieffer, and S. Q. Wang, J. Appl. Phys. **41**, 1199 (1970); J. R. Schrieffer, W. E. Evenson, and S. Q. Wang, J. Phys. (Paris) Colloq. **32**, C1-19 (1971).
[19] G. Morandi, E. Galleani D'Agliano, F. Napoli, and C. F. Ratto, Adv. Phys. **23**, 867 (1974).
[20] P. Soven, Phys. Rev. **156**, 809 (1967).
[21] H. Ehrenreich and L. M. Schwarz, Solid State Physics, edited by H. Ehrenreich, F. Seitz, and D. Turnbull (Academic, New York, 1976), Vol. 31, p.150.
[22] M.C. Gutzwiller, Phys. Rev. Lett. **10**, 159 (1963).
[23] M.C. Gutzwiller, Phys. Rev. **134**, A923 (1964).
[24] M.C. Gutzwiller, Phys. Rev. **137**, A1726 (1965).
[25] J. Hubbard, Proc. R. Soc. London A **276**, 238 (1963).
[26] J. Hubbard, Proc. Roy. Soc. London A **281**, 401 (1964).
[27] J. Kanamori, Prog. Theor. Phys. **30**, 275 (1963).
[28] Y. Kakehashi and P. Fulde, Phys. Rev. B **32**, 1595 (1985).
[29] H. Hasegawa, J. Phys. Condensed Matter **1** 9325 (1989).
[30] Y. Kakehashi, Phys. Rev. B **45**, 7196 (1992).
[31] Y. Kakehashi, Phys. Rev. B **65**, 184420 (2002).
[32] D.J. Amit and C.M. Bender, Phys. Rev. B **4**, 3115 (1971); D.J. Amit and H. Keiter, J. Low Temp. Phys. **11**, 603 (1973).
[33] Dai Xianxi, J. Phys. Condens. Matter. **3**, 4389 (1991).
[34] Y. Kakehashi, J. Phys. Soc. Jpn **77**, 094706 (2008).
[35] V.I. Anisimov, A.I. Poteryaev, M.A. Korotin, A.O. Anokhin, and G. Kotliar, J. Phys. Condens. Matter **9**, 7359 (1997).
[36] O.K. Andersen, O. Jepsen, and G. Krier, in *Methods of Electronic Structure Calculations* ed. by V. Kumar, O.K. Andersen, and A. Mookerjee (World Scientific Pub., Singapore, 1994) p. 63.
[37] Y. Kakehashi, M.A.R. Patoary, and T. Tamashiro, J. Phys. Soc. Jpn. **78**, 093705 (2009).
[38] Y. Kakehashi, M. Atiqur R. Patoary, and T. Tamashiro, Phys. Rev. B **81**, 245133 (2010).
[39] V.I. Anisimov, F. Aryasetiawan, and A.I. Lichtenstein, J. Phys. Condens. Matter **9**, 767 (1997).
[40] T. Bandyopadhyay and D.D. Sarma, Phys. Rev. B **39**, 3517 (1989).
[41] J.B. Mann, Los Alamos Scientific Laboratory Rep. No. LASL-3690 (1967).
[42] F. Aryasetiawan, K. Karlsson, O. Jepsen, and Schönberger, Phys. Rev. B **74**, 125106 (2006).
[43] T. Miyake and F. Aryasetiawan, Phys. Rev. B **77**, 085122 (2008).
[44] See for example, M. Imada and T. Miyake, cond-mat/1009.3851v1 (2010).
[45] Y. Kakehashi, Phys. Rev. B **66**, 104428 (2002).
[46] S. Hirooka and M. Shimizu, J. Phys. Soc. Jpn. **43**, 70 (1977).
[47] E. Müller-Hartmann, Z. Phys. B **74**, 507 (1989).
[48] M. Jarrell, Phys. Rev. Lett. **69**, 168 (1992); M. Jarrell and H.R. Krishnamurthy, Phys. Rev. B **63**, 125102 (2001).
[49] F.J. Ohkawa, Phys. Rev. B **46**, 9016 (1992).
[50] A. Georges and G. Kotliar, Phys. Rev. B **45**, 6479 (1992); A. Georges and W. Krauth, Phys. Rev. B **48**, 7167 (1993).
[51] A. Georges, G. Kotliar, W. Krauth, and M. J. Rozenberg, Rev. Mod. Phys. **68**, 13 (1996).
[52] Y. Kakehashi and P. Fulde, Phys. Rev. B **69**, 045101 (2004).
[53] O. Miura and T. Fujiwara, Phys. Rev. B **77**, 195124 (2008).
[54] A.I. Lichtenstein and M.I. Katsnelson, and G. Kotliar, Phys. Rev. Lett. **87**, 067205 (2001).
[55] Y. Kakehashi, J. Phys. Soc. Jpn., **50**, 1505 (1981); J. Phys. Soc. Jpn., **50**, 2251 (1981).
[56] S. Kirkpatrick, B. Velický, and H. Ehrenreich, Phys. Rev. B **1**, 3250 (1970).
[57] J. Korringa, J. Phys. Chem. Solids **7**, 252 (1958).
[58] H.J. Vidberg and J.W. Serene, J. Low Temp. Phys. **29**, 179 (1977).
[59] A.G. Narmonev and A.I. Zakharov, Phys. Met. Metallogr. **65**, 315 (1988).
[60] W. Speier, J.C. Fuggle, R. Zeller, B. Ackermann, K. Szot, F.U. Hillebrecht, and M. Campagna, Phys. Rev. B **30**, 6921 (1984).
[61] H.H. Potter, Proc. Roy. Soc. London **A 146**, 362 (1934).
[62] M. Fallot, J. de Phys. Rad. V, 153 (1944).
[63] Y. Barnier, R. Pauthenet, and L. Néel, Cobalt No. 21 (1963) (Cobalt Information Center).
[64] H.P. Myers and W. Sucksmith, Proc. Roy. Soc. **A 207**, 427 (1951).
[65] R.V. Colvin and S. Arajs, J. Phys. Chem. Solids **26**, 435 (1965).
[66] P. Weiss and R. Forrer, Ann. Phys. Paris **5**, 153 (1926).